Applied Surface Science 255 (2008) 2596–2602

Contents lists available at ScienceDirect

Applied Surface Science

journal homepage: www.elsevier.com/locate/apsusc

Characterization of rough interfaces obtained by boriding

I. Campos-Silva [a,*], A.S. Balankin [a], A.H. Sierra [b], N. López-Perrusquia [a], R. Escobar-Galindo [c], D. Morales-Matamoros [d]

[a] Instituto Politécnico Nacional, SEPI-ESIME, U.P. Adolfo López Mateos, Zacatenco, México D.F. 07738, Mexico
[b] Instituto Politécnico Nacional, UPIICSA, Av. Té 950, Col Granjas, México D.F. 08400, Mexico
[c] Instituto de Ciencia de Materiales de Madrid (CSIC), Cantoblanco, Madrid E-28049, Spain
[d] Instituto Mexicano del Petróleo, Eje Lázaro Cárdenas Norte, México D.F. 07738, Mexico

ARTICLE INFO

Article history:
Received 28 February 2008
Received in revised form 4 July 2008
Accepted 30 July 2008
Available online 3 August 2008

Keywords:
Boriding
Interfaces
Self-affine and multi-affine fractals
Roughness
Hurst exponent
Universal multi-fractals

ABSTRACT

This study evaluates the morphology of borided interfaces by means of the fractal theory. The boride layers were formed in the AISI M2 steel by applying the paste boriding treatment at temperatures of 1253 and 1273 K and treatment times of 2 and 6 h, while a boron carbide paste thickness of 4 or 5 mm covered the samples surface in order to produce the boron diffusion. The morphology of interfaces formed between FeB and Fe_2B layers and between Fe_2B layer and steel substrate was analyzed by the rescaled-range (R/S), root-mean-square (RMS), and Fourier power spectrum (FPS) methods. Moreover, the multi-affine spectra of roughness exponent were obtained by calculating the q-order height–height correlation functions. We found that both interfaces are multi-affine, rather than self-affine. The multi-affine spectra of roughness exponents are found to be different for FeB/Fe_2B and Fe_2B/substrate interfaces, but independent on the treatment parameters (boron carbide paste thickness, temperature, and boriding time). Furthermore, we found that the multi-affine spectra of both interfaces behave as it is expected for "universal multi-fractals" with the Lévy index $\gamma = 1$, associated with the multiplicative cascades with a log-Cauchy distribution. Furthermore, our data suggest a great homogeneity of the boron diffusion field, characterized by universal fractal dimension $D_{diff} = 2.90 \pm 0.01$. These findings provide a novel insight into the nature of phase formation during the boriding treatment.

1. Introduction

Boriding is the surface boron saturation of metals and alloys with the purpose of increasing their hardness, wear and corrosion resistance in engineering components where their industrial applications require those properties [1,2]. One of the most interesting topics in the field of boriding process during the last 20 years is concerned with the growth kinetics of boride layers [3–10]. The growth of rough surfaces and interfaces plays a major role in many phenomena of scientific interest and practical importance [11–15]. Early, it was found that the interfaces FeB/Fe_2B and Fe_2B/substrate, which are present at the surface of different ferrous and non-ferrous alloys in boriding processes, have a rough or saw-toothed morphology [1–4]. However, when the alloying elements increase on the substrate, the formation and morphology of the growth interface at the surface of the sample tends to be flat [16–18]. Recently, significant progress in understanding layers' microstructure is derived by applying the methods of statistical mechanics, especially the modern concept of scaling, to the space and the time evolution of surface morphology (see [11–15] and references therein). The dynamics of interfaces ranging from vapor deposition to fluid invasion in porous media can often be described by relatively simple evolution equations [13–17]. Typically the evolution equations are given in terms of partial differential equations with a stochastic noise component, such as the seminal Kardar–Parisi–Zhang (KPZ) equation [19], which describes kinetic roughening of randomly driven interfaces such as molecular-beam epitaxy or anomalous diffusion in disordered media and wetting phenomena [12]. The dynamical scaling associated with the height fluctuations on growing surfaces implies generic scaling invariance, both spatially and temporally [11–15]. Such scale invariance is quantified by critical exponents that characterize these fluctuations. Often, the interfaces reveal self-similar or self-affine geometry [11–15]. The roughness of a self-similar surface is isotropically scaleable, that is the roughness is invariant under similarity transformation $x \to bx$, $y \to by$, and $z \to bz$, where b is the positive scaling factor [20]. In contrast to this, the roughness

* Corresponding author. Tel.: +52 55 57296000x54768; fax: +52 55 57296000x54589.
E-mail address: icampos@ipn.mx (I. Campos-Silva).

0169-4332/$ – see front matter © 2008 Elsevier B.V. All rights reserved.
doi:10.1016/j.apsusc.2008.07.142

of a self-affine surface displays intrinsically anisotropic scaling, such that to keep scaling invariance the changes along the surface, $x \to bx$, $y \to by$, should be accompanied by the rescaling $z \to b^H z$ in the normal direction. So, $z(bx,by) = b^H z(x,y)$,[1] where the exponent H is called the Hurst exponent [20].

For self-similar surfaces $H = 1$, whereas for self-affine surfaces the value of Hurst exponent is in the range $0 \leq H < 1$ [20]. In the last case, the Hurst exponent gives an indication of whether the system behavior is random or possesses long-range power law correlations [20–23]. A Hurst exponent of $H = 0.5$ corresponds to ordinary uncorrelated Brown motion. If $0.5 < H < 1$, the surface displays persistence and characterized by positive long-range correlation, i.e., a trend (for example, a high or low value) at $r = (x,y)$ is likely to be followed by a similar trend at $r + \Delta r$, whereas if $H > 0.5$, the surface is antipersistent, i.e., a trend at r is not likely to be followed by a similar trend at $r + \Delta r$ [20–23]. Furthermore, it was shown that for non-intersecting self-affine surfaces the Hurst exponent is related to the box-counting fractal dimension of surface D_B as $H = (d + 1) - D_B$, where d is the topological dimension of surface [20–23]. So, the lower is the Hurst exponent, the more space invasive is the surface [20–23].

Rough interfaces occurring in nature are usually one-dimensional profiles ($d = 1$) or surfaces ($d = 2$). In practice, the roughness of two-dimensional surfaces is commonly studied through the analysis of their one-dimensional profiles $h(x,t)$ obtained by the intersection of the surface with a normal plane.[2] Once we have scaled down the analysis to (1 + 1) dimensions, the surface roughness can be characterized by the fluctuations of the surface height around its mean value. In this way, at the time moment t the global roughness of surface is quantified by the root-mean-square (RMS) fluctuation of the surface height, $W(L,t) = \langle [h(x,t) - \langle h(x,t)\rangle_L]^2\rangle_L$, which is the standard deviation of $h(x,t)$ from its mean value $\langle h(x,t)\rangle_L$ in the system of size L; the brackets denote average over all $0 \leq x \leq L$ [11–15]. Additionally, the local morphology of surface can be characterized by the local width of fluctuations within a sampling interval (windows) along the horizontal direction of size Δx, defined as

$$\sigma(\Delta x, t) = \langle \langle [h(x,t) - \langle h(x,t)\rangle_{\Delta x}]^2 \rangle_{\Delta x} \rangle_R, \tag{1}$$

where $\langle \cdots \rangle_{\Delta x}$ denotes an average over x in sampling interval of size Δx and $\langle \cdots \rangle_R$ denotes an average over different realizations along the profile of length L [12]. One can see that per definition $W(L,t) = \sigma(\Delta x = L,t)$.

It was found that the kinetic roughening of growing interfaces frequently obeys the celebrated Family–Vicsek dynamic scaling ansatz [44]:

$$W(L,t) = t^{\alpha/z} f\left(\frac{L}{\xi(t)}\right), \tag{2}$$

where the asymptotic behavior of the scaling function $f(y)$ is constant for $y \gg 1$ and scales as y^α for $y < 1$ with the so-called global roughness exponent α, while the horizontal correlation length $\xi(t)$ behaves as $\xi \propto t^{1/z}$, where z is called the dynamic exponent [11–15]. So, at the initial stage, $\xi(t) \ll L$ and the global width of interface increases with time as $W(L,t) \propto t^\beta$, where $\beta = \alpha/z$ is termed as the growth exponent [11–15], whereas in the (quasi)stationary regime, $\xi(t) \geq L$ and the global width of interface grows with the system size as $W(L,t) \propto L^\alpha$ [11–15].

It is easy to understand that for self-affine surfaces $\alpha = H$, whereas for a self-similar surface $\alpha = 1$ [15,45]. Moreover, for self-similar and self-affine surfaces it is expected that the local width, $\sigma(\Delta x,t)$, also satisfies the Family–Vicsek dynamic scaling ansatz with the same scaling exponents [11–15]. So, the dynamic of self-affine and self-similar surfaces is characterized by only two independent scaling exponents: H and z, in the case of self-affine surfaces, and the fractal dimension D_B and the dynamic scaling exponent $z = 1/\beta$, in the case of self-similar surfaces [11–15]. These exponents determine the universality class of kinetic roughening process under consideration.[3]

While the self-affine and self-similar roughness of growing interfaces was observed in many physical systems (see [11–15]), more generally, the scaling behavior of local surface width, $\sigma(\Delta x) \propto (\Delta x)^{\zeta_2}$, is characterized by the local roughness exponent ζ_2, which is less or equal to the global roughness exponent, i.e., $\zeta_2 \leq \alpha$ [47–54]. The case of $\zeta_2 = \alpha = H$ corresponds to self-affine (or self-similar, if $\zeta_2 = \alpha = H = 1$ [45]) surfaces, whereas surface roughness characterized by $\zeta_2 < \alpha$ is termed as an "anomalous" roughness [47] and it is characterized by three or more independent scaling exponents, e.g., ζ_2, α, and z, etc. [24–28]. The generic dynamic scaling ansatz for "anomalous" kinetic roughening and the classification of its regimes were suggested in [24] (see also [25–30]). The set of independent scaling exponents determines the universality class of the corresponding anomalous roughening process [11–15,46].

The Family–Vicsek and generic scaling dynamics are observed in a grain variety of physical systems [11–30]. However, in many cases the local geometry of the interface is not pure self-similar or self-affine, rather than multi-fractal [20,22,23,55–58] or multi-affine [59–65]. The multiscaling properties of such interfaces can be investigated by calculating the q-order height–height correlation function defined as

$$G_q(\Delta x) = \frac{1}{N}\sum_{i=1}^{N} |h(x_i) - h(x_i + \Delta x)|^q, \tag{3}$$

where $N \gg 1$ is the number of points along interface over which the average is taken [59,60]. For surfaces with the long-range correlations in height fluctuations the q-order height–height correlation functions generally obey the scaling behavior

$$G_q(\Delta x) \propto (\Delta x)^{q\zeta_q}, \tag{4}$$

with ζ_q changing continuously with q at least for some regions of the q values [59–65], such that per definition $\zeta_1 = H$ [20] and so, for a self-affine surface $\zeta_q = H$ for any q [59].

It should be pointed out that the multi-affine scaling can be caused by the removal of overhangs in the representation of real interface by single-valued profile [66] or can has an intrinsic nature, associated with the physical nature of roughening kinetic [62–65,67–70] To distinguish between these reasons for multi-

[1] Real surfaces can be self-affine only in a statistical sense and so, the relation should be replaced by $z(bx,by) \cong b^H z(x,y)$, where symbol $\cong$ means the statistical equality [20]. Furthermore, in most of the physical self-affine surfaces, the scale invariance does not extend to all length scales but there are a lower l_0 and an upper ξ cutoffs below and above of which the surface is no longer correlated [20,21]. The lower cutoff is determined by the material microstructure [21,22]. The length at which the upper cutoff appears is defined as the correlation length [20–22].

[2] Most of the methods used for determination of self-affine invariance are devoted to uni-valued (1 + 1) dimensional profiles [20–41]. So, the overhangs observed for many rough surfaces are commonly neglected or treated in some manner to obtain the uni-valued representations of multi-valued profiles (see [42]). The particular case of in-plane anisotropy results in a dependence of H on the orientation of the plane with respect to the surface [22,43].

[3] The important result of the kinetic roughening studies is that a large variety of different growth models can be divided into only a few universality classes (see Refs. [11–15,46] and references therein). The dynamical universality classes are determined by the system dimensionality, the conservation laws, the symmetry of the order parameter, the range of the interactions, and the coupling of the order parameter to conserved quantities [46]. It was found that many interfaces observed in different physical experiment belong to one of the universality classes predicted in the theory of kinetic roughening (see [11–15] and references therein).

affinity, we need to study the functional behavior of ζ_q-spectrum. In the case of vertical discontinuities produced by the neglection of overhangs, it is expected (see [66]) that for sufficiently larger q the spectrum behaves as $\zeta_q \propto 1/q$, whereas in the more interesting case of physical multi-affinity associated with the multiplicative cascades in the process of interface formation, the spectrum of scaling exponents is expected to obey a universal scaling behavior [67–70]:

$$\zeta_q = \begin{cases} H - \dfrac{c}{\alpha - 1}(q^{\gamma-1} - 1) & \text{when } 1 < \gamma \neq 1 \leq 2 \\ H - c\ln(q) & \text{when } \gamma = 1 \end{cases}, \quad (5)$$

termed as the "universal multi-fractal", where c is an intermittency parameter called the mean fractal inhomogeneity measure and γ is the Lévy index which characterizes the degree of multi-fractality [67–70]. The Lévy index γ determines the type of probability distribution for the extreme statistics. Theoretically, it varies between 0 and 2 and indicates how far the kinetic roughening is from a self-affine process. The case of $\gamma = 0$ corresponds to self-affine surfaces, $\gamma = 1$ is related to a log-Cauchy distribution of multiplicative cascade, while $\gamma = 2$ is associated with lognormal multi-affinity [67–70]. It is essential to note that the intermittency parameter measures intrinsically the fraction of space occupied by active elements, i.e., its relative sparseness [67]. It was shown that c is equal to the co-dimension of mean singularity of multi-fractal field, i.e.,

$$c = d_E - D_f \quad (6)$$

where D_f is the fractal dimension of field and d is the topological dimension of emending space [67–70]. So, for homogeneous processes $c = 0$, whereas $c = d_E$ for a process so heterogeneous that the fractal dimension of the set to the mean is zero [67–70]. Some other physical mechanisms leading to intrinsic multi-affinity of growing surfaces were studied in references [71–73,70].

Unfortunately, theoretical understanding of interface dynamics in real experimental situations remains problematic. The existing theoretical models of surface growth apply to a very limited set of experiments. So, the kinetic roughening model to be applied, we need to analyze the scaling properties of interfaces under the study, because an accurate knowledge of roughness exponents is required to take a deep insight on the underlying formation processes (see [11–15]).

In this work we study the roughness of interfaces formed in the boriding processes. The purpose of this study is to characterize the morphology of the borided layers created at the surface of AISI M2 steels using the fractal techniques of kinetic roughening theory.

2. Experimental procedures

The growth of monophase or polyphase boride layers depends essentially on the substrate chemical composition, the boron potential that surrounds the material, the temperature, and the treatment time [5–7]. In this work, the paste boriding treatment was carried out on AISI M2 steel. Early, it was found that in this steel, two phases can form depending on the boron potential, the substrate temperature and treatment time: the outer phase FeB, with a boron content of ~16 wt.%, and an inner phase Fe_2B, with a boron content of ~9 wt.% (see [3,4]). The morphology displayed by both layers is saw-toothed, with a columnarity extent of the layer–substrate interface which mainly depends on the nature and amount of alloying elements in the steel [3,4]. Notice that, generally, the boride–steel interface tends to be columnar for low or medium carbon steels and flat for high alloy steels [4,74]. In this work, the roughness of FeB/Fe_2B and Fe_2B/substrate interfaces formed in the AISI M2 steel were studied using the photo images of vertical cross-sections of samples after boriding treatment (see [4]).

Table 1
Global width and roughness exponents (error bars correspond to the standard deviation among five values) of interfaces between the FeB and Fe_2B phases and between the Fe_2B phase and steel substrate for specimens subjected to different boriding treatments

	Treatment[a]	W, μm	H	ζ_2	α_S
FeB/Fe_2B	1	3.8	0.75 ± 0.03	0.69 ± 0.04	0.67 ± 0.05
	2	5.1	0.75 ± 0.02	0.70 ± 0.03	0.68 ± 0.05
	3	5.7	0.75 ± 0.02	0.70 ± 0.02	0.69 ± 0.05
	4	5.7	0.75 ± 0.02	0.70 ± 0.03	0.70 ± 0.05
	5	8.2	0.75 ± 0.01	0.70 ± 0.02	0.70 ± 0.05
Fe_2B/steel	1	7.3	0.94 ± 0.03	0.86 ± 0.02	0.81 ± 0.06
	2	10.7	0.94 ± 0.03	0.87 ± 0.02	0.85 ± 0.06
	3	11.2	0.94 ± 0.02	0.85 ± 0.02	0.85 ± 0.06
	4	11.3	0.94 ± 0.02	0.86 ± 0.02	0.85 ± 0.06
	5	17.6	0.94 ± 0.02	0.86 ± 0.02	0.85 ± 0.06

[a] Boriding treatments: (1) 2 h with 5 mm paste at 1253 K, (2) 6 h with 5 mm paste at 1253 K, (3) 2 h with 5 mm paste at 1273 K, (4) 4 h with 4 mm paste at 1273 K, and (5) 6 h with 5 mm paste at 1273 K.

2.1. Boriding process

For boriding treatment we used the rectangular AISI M2 steel samples with size of 20 mm × 20 mm × 0.5 mm, which were introduced into a conventional furnace under pure argon atmosphere at the temperatures of 1253 and 1273 K. The exposure times were 2 and 6 h, while a boron carbide paste[4] of thickness 4 and 5 mm was used to cover one side of the material surface (see, for details [3,4]). Considering that the used boron potentials were similar to those in the work [4], the influence of alloying elements in the AISI M2 steel, causes the formation of two phases: FeB and Fe_2B (see [4]). Both phases show a preferential growth over plane (0 0 2) [4]. The dependence of the process on time and temperature, results in an increase of the layer thickness with temperature and treatment time [3]. The growth kinetics of the borided phases, FeB and Fe_2B, is also dependent of the paste boron carbide thickness over the substrate surface [4]. It was also noted that as the boron potential increases, the layers become more compact and continuous [4].

In this work, at the end of the boriding treatment, each sample was quenched in oil, cross-sectioned by electrical discharge machining, and than prepared metallographically[5] for its characterization using an Olympus GX51 optical microscope with the 400× magnification. The thickness of the boride layers (see Table 1) was measured by means of optical microscopy in clear field.[6]

2.2. Images processing

The cross-sections of all samples were optically sectioned, and the photo images of all sections of width 161 μm were acquired with the resolution of 13 pixel/μm, such that each image has the width of 2048 pixels[7] (see Fig. 1(a)). The chemical composition of the upper (FeB) and lower (Fe_2B) layers were determined in the early works [3,4] by the XRD analysis using Co Kα radiation with λ = 1.54 Å. In this work, to evaluate the local morphology of the growing interfaces, five photo images of width of 2048 pixels each were selected randomly from the cross-section of each sample.

[4] The boron carbide paste ($B_4C + Na_3AlF_6$) was mixed with distilled water with a 0.2 ratio (boron carbide paste/water).

[5] The metallographic preparation employed a sequence of abrasion, until 1000-grit silicon carbide paper, followed by polishing with a diamond paste and ethylene glycol.

[6] In each sample, a minimum of 25 measurements were done at different points; the reported values are the thickness layers average (see also [4]).

[7] To determine the global widths of interfaces, the full images of each cross-section were reconstructed from corresponding image series.

These images were binarized using a conventional software for this purpose (see Fig. 1(b)), and then digitized with the help of the Scion Image Beta 4b software [75] to obtain the single-valued slice series $h(x_i)$[8] of the FeB/Fe_2B and Fe_2B/substrate interfaces (see Fig. 1(c)), which were further used for the roughness analysis.

3. Roughness analysis methods

An accurate estimation of scaling exponents characterizing a rough surface has deep physical implications and is of crucial importance for the identification of the universality class of the kinetic roughening phenomena [11–15,46]. There are many methods to measure the scaling exponents of rough profiles, such as the rescaled-range (R/S), roughness length (the RMS-roughness), variogram (the height–height correlation function scaling), detrended fluctuation analysis (DFA), return probability scaling (RPS), diffusion entropy analysis (DEA), Fourier power spectrum (FPS), and wavelet methods, among others (see [22–42] and references therein). Each method has its advantages and disadvantages. The reliability of different methods of roughness analysis was discussed in the works [24–34]. In this work, we used the rescaled-range analysis, roughness length scaling, Fourier power spectrum method, and multi-affine analysis based on the scaling behavior of q-order height–height correlation functions $G_q(\Delta x,t)$.

3.1. Rescaled-range analysis

We begun our investigation with oldest classic method called the rescaled-range analysis. This method, proposed by Mandelbrot and Wallis [36] and based on previous hydrological analysis of Hurst [35], allows the calculation of the Hurst exponent H. The basis of the method is that, because of self-affinity, one expects the range taken by the values of $h(x)$ in a window of length Δx to be proportional to the window length to a power equal to the Hurst exponent. A reliable measurement of R/S requires data with a constant sampling interval Δx. In this work, a rough interface is represented by discrete univalued profile $h(x_i)$, where $1 \le i \le N = 2048$, such that $x_1 = 0$ and $x_{2048} = 161$ μm. So, the rescaled-range $R/S = f(n)$ for $2 \le n \le 2048$ is calculated as

$$R/S = \frac{1}{\sigma(n)} \times \left\{ \max_{1\le k\le n}\left[\sum_{j=1}^{k}(h(x_j) - \langle h\rangle_n)\right] - \min_{1\le k\le n}\left[\sum_{j=1}^{k}(h(x_j) - \langle h\rangle_n)\right]\right\}, \quad (7)$$

where

$$\langle h\rangle_n = \frac{1}{n}\sum_{i=1}^{n} h(x_i) \text{ and } \sigma(n) = \left[\frac{1}{n}\sum_{j=1}^{n}(h(x_j) - \langle h\rangle_n)^2\right]^{1/2} \quad (8)$$

are the sample mean and standard deviation, respectively. For surfaces with the long-range correlations the rescaled-range is expected to scale with the window size n[9] as

$$\frac{R}{S} \propto n^H. \quad (9)$$

Accordingly, the Hurst exponent can be obtained from the linear part of the log–log plot of R/S versus n. The relative power of rescaled-range analysis versus alternative methods of estimating the Hurst exponent for fractional Gaussian processes has been recently studied in works [76–78]. The sampling properties of R/S estimates of the Hurst exponent were studied by Ellis [34], who has determined the confidence intervals for the statistical significance of the Hurst exponent obtained by R/S method.

3.2. The roughness length method

The roughness length method explores the scaling behavior of the RMS roughness, which represent the local interface width (1) of interface, defined as the standard deviation of $h(x_i)$ in the window

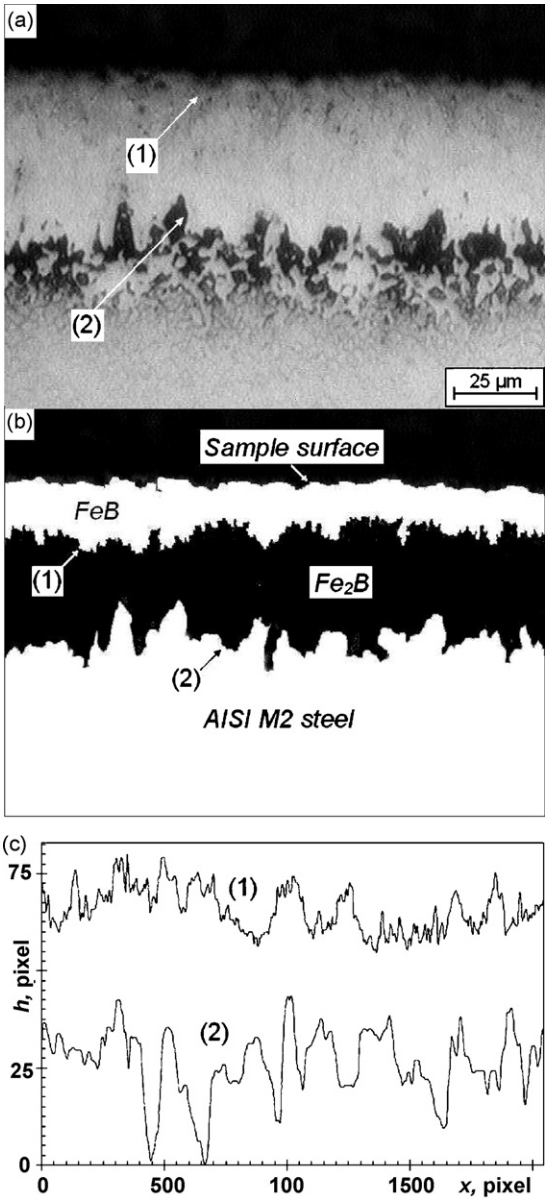

Fig. 1. Image processing: (a) cross-sectional view with 400× magnification of AISI M2 steel after the boriding treatment with a boron carbide paste thickness of 5 mm at 1253 K during 6 h; (b) binarized image of interfaces, and (e) digitized graphs $h(x)$ of interfaces between the FeB and Fe_2B phases (1) and between the Fe_2B layer and AISI M2 steel (2).

[8] While analyzing a profile $h(x)$, we represent it as a discrete series of points $h(x_i)$, where $x_{i+1} - x_i = 1$ pixel and $1 \le i \le N = 2048$.

[9] The original specification of the classical rescaled range provided by Hurst [35] was such that the roughness exponent was estimated for the whole sample length N. The procedure was later modified by Mandelbrot and Wallis [36] to incorporate ordinary least squares (OLS) regression techniques where the exponent (denoted H by Mandelbrot and Wallis) was estimated over several sub-series $n < N$.

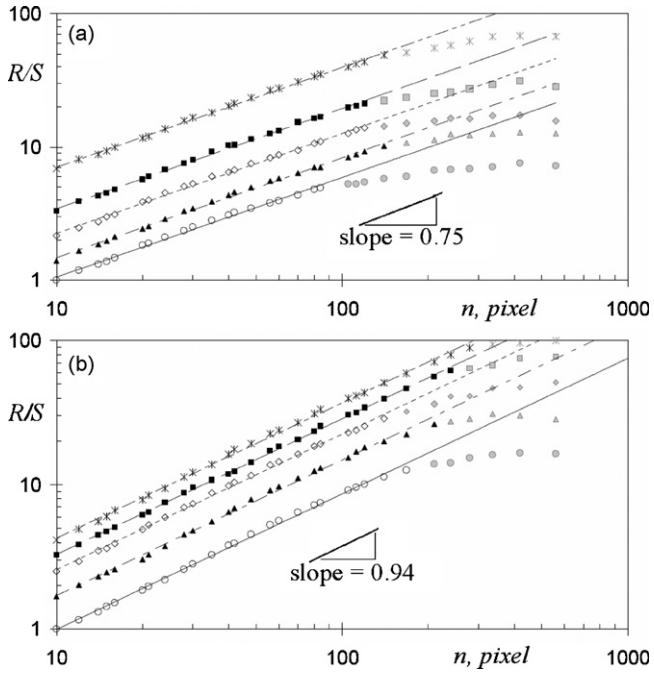

Fig. 2. Log–log plots of the rescaled-range (R/S in arbitrary units) versus the window size (n in pixels) for interfaces between: (a) FeB and Fe_2B phases and (b) Fe_2B layer and AISI M2 steel in specimens treated: 2 h with 5 mm paste at 1253 K (circles); 6 h with 5 mm paste at 1253 K (triangles); 2 h with 5 mm paste at 1273 K (rhombus); 6 h with 4 mm paste at 1273 K (squares); and 6 h with 5 mm paste at 1273 K (crosses). Symbols, experimental data averaged over five images from each sample; straight lines, the minimum root square fittings according to the scaling behavior (9); the grey symbols are excluded from fitting. Notice that the graphs are shifted along the X-axis to clarity.

of size $\Delta x = n$ (second equation in (7)). In this work, for a given window length, the input series is subdivided in a number $(N - n)$ of intervals of length $2 \leq n < 2048$ and the standard deviation is calculated in each window after subtracting a local linear trend. The final estimate is taken to be the average (1) of RMS roughness for the windows of the same size n. Accordingly, the local roughness exponent ζ_2 is defined as the slope of the linear part of the log–log plot of $\sigma(\Delta x = n)$ versus n. Notice that $\zeta_2 = H$ only for self-affine (or self-similar $\zeta_2 = H = 1$) surfaces [20]. So, the inequality $\zeta_2 \neq H$ indicates the lack of self-affinity. In such a case, the multi-affine analysis should be performed.

3.3. Height–height correlations analysis

The multi-scaling properties of interfaces in this work were studied by calculating the q-order height–height correlation function, $G_q(\Delta x = n)$, defined by the Eq. (3). The spectrum of scaling exponents ζ_q was determined for each interface by linear fitting of log–log plots of G_q versus n (see Eq. (4)) for $1 \leq q \leq 10$ For a self-similar or self-affine surface ζ_q is independent of q whereas for a multi-affine surface it depends on q. In the last case, to determine the reason of multi-affine behavior we studied the functional behavior of ζ_q on q using the mean square best fit of the experimental values.

3.4. Fourier power spectrum analysis

In this work, the interface roughness was also characterized by calculating the structure factor or power spectrum, $S(k) = \langle Z(k)Z(-k)\rangle_R$, where $Z(k)$ is the Fourier transform of the height of the surface $h(x_i)$ in a section of size $N = 2048$, which is given by the equation

$$Z(k) = N^{-1/2}\sum_{i=1}^{N}[h(x_i) - \langle h(x_i)\rangle_L]\exp(ikx_i) \tag{10}$$

where the spatial average of the height has been subtracted; k is the wave number. Generally, the power spectrum of a rough interface is expected to scale as

$$S(k) \propto k^{-(2\alpha_S+1)} \tag{11}$$

where for multi-affine surfaces, the spectral roughness exponent α_S is equal to ζ_2 [2]. So, for a self-affine interface, whereas for multi-affine interfaces $\alpha_S = \zeta_q \neq H$. However, for interfaces with "anomalous" roughness (see [47,48]) the spectral roughness exponent may be an independent characteristic of surface roughness, i.e., $\alpha_S \neq \zeta_2$ [47]. In this work, the power spectrum analysis was performed with the help of commercial BENOIT 1.3 software [79].

4. Results and discussion

Fig. 2(a) and (b) shows the log–log plots of R/S versus n for the FeB/Fe_2B and Fe_2B/substrate interfaces, respectively. One can see that the Hurst exponents of these interfaces are independent on the treatment parameters (boron carbide paste thickness, temperature and time of treatment), while the FeB/Fe_2B and Fe_2B/substrate interfaces are characterized by the different Hurst exponents (see Table 1). This indicates that the kinetics of FeB and Fe_2B phase formations belong to different universality classes (see [11–15]).

The local roughness exponent is also found to be different for the FeB/Fe_2B and Fe_2B/substrate interfaces, while in both cases the local roughness exponent is independent on the treatment parameters and less than the corresponding Hurst exponent (see Fig. 3 and Table 1). The inequality $\zeta_2 < H$ indicates than the roughness of interfaces is multi-affine, rather than self-affine.

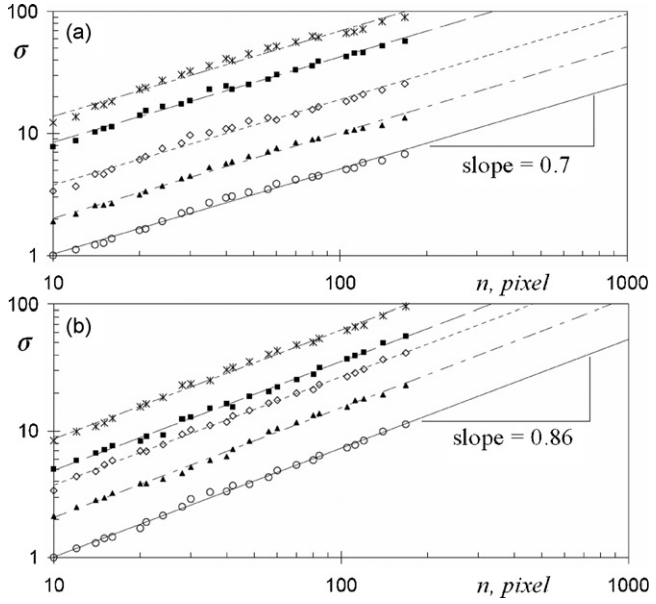

Fig. 3. Log–log plots of the RMS-roughness ($\sigma(n)$ in arbitrary units) versus the window size (n in pixels) for interfaces: (a) between the FeB and Fe_2B phases and (b) between the Fe_2B layer and AISI M2 steel in specimens treated: 2 h with 5 mm paste at 1253 K (circles); 6 h with 5 mm paste at 1253 K (triangles); 2 h with 5 mm paste at 1273 K (rhombus); 6 h with 4 mm paste at 1273 K (squares); and 6 h with 5 mm paste at 1273 K (crosses). Symbols, experimental data; straight lines, the minimum root square fittings according to the scaling behavior $\sigma(\Delta x = n) \propto n^{\zeta_2}$. Notice that grey symbols are excluded from fitting.

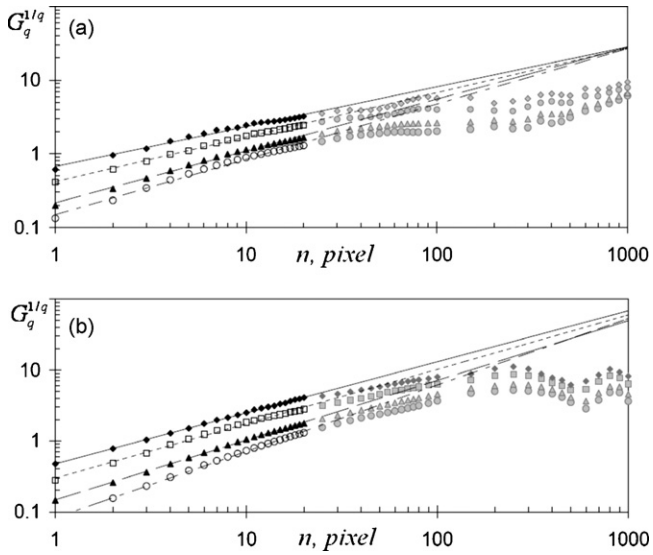

Fig. 4. Log–log plots of $G_q^{1/q}(n)$ versus n for $q = 1$ (circles), 2 (triangles), 5 (squares), and 10 (rhombus) for the interface between: (a) FeB and Fe_2B phases and (b) Fe_2B layer and AISI M2 steel in the sample treated with a boron carbide paste thickness of 5 mm at 1273 K during 6 h. Symbols, experimental data; straight lines, the minimum root square fittings according to the relation (4). Notice that grey symbols are excluded from fitting.

Accordingly, the multi-affine spectrum ζ_q of each interface was calculated according to the scaling behavior (4) (see Fig. 4). As it is expected for multi-affine interfaces, we found that for each interface $\zeta_1 = H < \zeta_2$. Furthermore, all scaling exponents ζ_q are found to be independent on the treatment parameters and for both interfaces obey a universal behavior

$$\zeta_q = H - c\ln(q) \tag{12}$$

with the same intermittency parameter

$$c = 0.093 \pm 0.007 \tag{13}$$

for the FeB/Fe_2B and Fe_2B/substrate interfaces (see Fig. 5). We noted that this behavior coincides with those expected for universal multi-fractals (5) with the Lévy index $\gamma = 1$, corresponding to a log-Cauchy distribution of multiplicative cascades (see [67–70]).

Finally, we studied the Fourier power spectra of interfaces (see Fig. 6). We found that in all cases the spectral roughness exponent α_S is equal to the corresponding local roughness exponent, ζ_2, as it is expected for multi-affine surfaces (see Table 1).

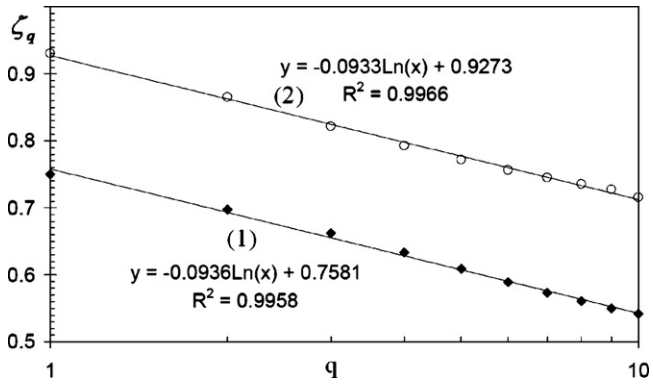

Fig. 5. The graphs of multi-affine spectra (ξ_q versus $\log q$) for interfaces between the FeB and Fe_2B phases (1) and between the Fe_2B layer and AISI M2 steel (2). Symbols, experimental data averaged over all samples (25 values); straight lines, the minimum root square fittings according to the relation (12).

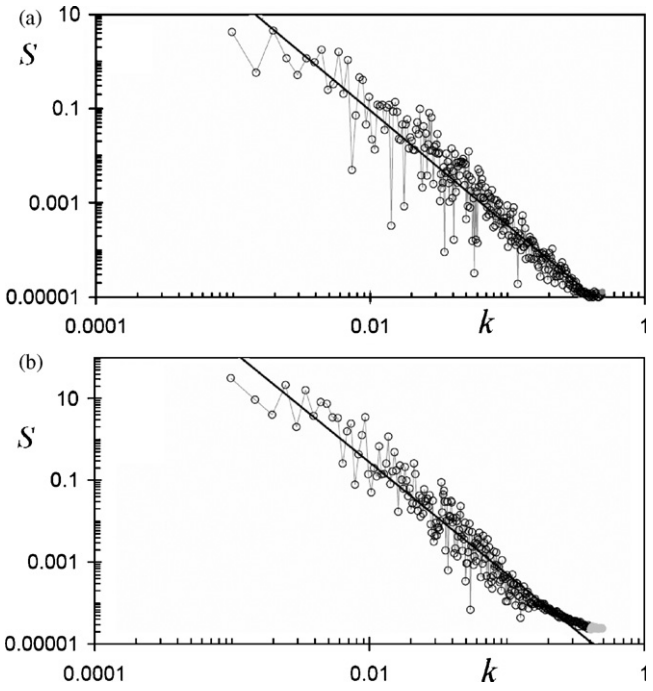

Fig. 6. Log–log plots of the Fourier power spectra (S in arbitrary units) versus the wavenumber (k in 1/pixel) of interfaces between (a) FeB and Fe_2B phases and (b) Fe_2B layer and AISI M2 steel in the sample treated with a boron carbide paste thickness of 5 mm at 1253 K during 6 h. Circles, experimental data; straight lines, the minimum root square fittings according to the scaling behavior (11).

5. Conclusions

We studied the roughness of interfaces between the FeB and Fe_2B layers and between the Fe_2B layer and the substrate (steel) formed during the boriding treatment of AISI M2 steel. Our findings suggest that both interfaces are multi-affine, rather than self-affine. While the width of FeB and Fe_2B layers, as well as the width of interfaces, are strongly dependent on the treatment parameters, such as the boron carbide paste thickness, temperature, and time (see Table 1), both interfaces display the universal[10] scaling properties obeying the universal multi-fractal scaling behavior (11). However, the interface between FeB and Fe_2B layers is more space invasive than the interface between Fe_2B and substrate, nevertheless the last has the larger width. These findings provide a novel insight into the nature of phase formation during the boriding treatment. Specifically, universal behavior of multi-affine spectra suggests that the interfaces arise as outcomes of a multiplicative stochastic boron diffusion process governed by the Lévy stable log-Cauchy probability distribution. At the same time, a small value of intermittency parameter (13) indicates a great homogeneity of the boron diffusion field, characterized by the fractal dimension $D_{\text{diff}} = 3 - c = 2.9 \pm 0.01$ (see Eqs. (6) and (13)).

Acknowledgments

This work has been supported by the research grant 53859 of *Consejo Nacional de Ciencia y Tecnología* at Mexico. I. Campos thanks the project *20080048* chair supported by the *Secretaría de Investigación y Posgrado* of the Instituto Politécnico Nacional.

[10] In the sense that roughness exponents are independent on the treatment parameters, at least in the range used in this work.

References

[1] A. Graf von Matuschka, Boronising, Carl Hanser Verlag, Munich, FRG, 1980.
[2] I. Campos, M. Islas, G. Ramírez, C. Villa Velázquez, C. Mota, Appl. Surf. Sci. 253 (2007) 6226–6231.
[3] I. Campos, O. Bautista, G. Ramírez, M. Islas, J. de la Parra, L. Zúñiga, Appl. Surf. Sci. 243 (2005) 429–436.
[4] I. Campos, R. Torres, O. Bautista, G. Ramírez, L. Zuñiga, Appl. Surf. Sci. 252 (2006) 2396–2403.
[5] S. Sen, U. Sen, C. Bindal, Surf. Coat. Technol. 191 (2005) 274–285.
[6] C.M. Brakman, A.W.J. Gommers, E.J. Mittemeijer, in: Proceedings of Heat Treatment 88, The Institute of Metals, 1988, pp. 211–217.
[7] V.I. Dybkov, W. Lengauer, P. Gas, J. Mater. Sci. 41 (2006) 4948–4960.
[8] L.G. Yu, X.J. Chen, K.A. Khor, G. Sundararajan, Acta Mater. 53 (2005) 2361–2368.
[9] E. Meléndez, I. Campos, E. Rocha, M.A. Barrón, Mater. Sci. Eng. A234–236 (1997) 900–903.
[10] L.G. Yu, K.A. Khor, G. Sundararajan, Surf. Coat. Technol. 201 (2006) 2849–2853.
[11] T. Vicsek, Fractal Growth Phenomena, World Scientific, Singapore, 1992.
[12] P. Meakin, The growth of rough surfaces and interfaces, Elsevier Science Publishers B.V., Netherlands, 1993.
[13] V.S. Ivanova, A.S. Balankin, I.Zh. Bunin, A.A. Oksogoev, Sinergetics and Fractals in Materials Science, Nauka, Moscow, 1994.
[14] A.-L. Barabási, H.E. Stanley, Fractal Concepts in Surface Growth, Cambridge University Press, 1995.
[15] P. Meakin, Fractals, Scaling and Growth Far from Equilibrium, Cambridge University Press, 1998.
[16] A.K. Sinha, Boronizing, ASM Handbook, OH, USA, J. Heat Treat. 4 (1991) 437.
[17] S.C. Singhal, Thin Solid Films 45 (1977) 321–329.
[18] R. Buzio, A. Chierichetti, G. Bianchi, U. Valbusa, Surf. Coat. Technol. 200 (2006) 6430–6433.
[19] M. Kardar, G. Parisi, Y.C. Zhang, Phys. Rev. Lett. 58 (1987) 2087–2090.
[20] B.B. Mandelbrot, The Fractal Geometry of Nature, W. H. Freeman and Company, New York, 1999.
[21] A.S. Balankin, Eng. Fract. Mech. 57 (1997) 135–203.
[22] A.S. Balankin, F.J. Sandoval, Rev. Mex. Phys. 43 (1997) 545–591.
[23] J.G. Moreirat, J.K. Leal da Silva, S.O. Kamphors, J. Phys. A: Math. Gen. 27 (1994) 8079–8089.
[24] J. Schmittbuhl, J.-P. Vilotte, S. Roux, Phys. Rev. E 51 (1995) 131–147.
[25] A.R. Mehrabi, H. Rassamdana, M. Sahimi, Phys. Rev. E 56 (1997) 712–722.
[26] H.-N. Yang, Y.-P. Zhao, A. Chan, T.-M. Lu, G.-C. Wang, Phys. Rev. B 56 (1997) 4224–4232.
[27] P.H.S.W. Kulatilake, J. Um, G. Pan, Int. J. Solid Struct. 35 (1998) 4167–4189.
[28] J. Buceta, J. Pastor, M.A. Rubio, F.J. de la Rubia, Phys. Rev. E 61 (2000) 6015–6018.
[29] G. Rangarajan, M. Ding, Phys. Rev. E 61 (2000) 4991–5001.
[30] K. Hu, P.Ch. Ivanov, Zh. Chen, P. Carpena, H.E. Stanley, Phys. Rev. E 64 (2001), 011114/1–011114/19.
[31] G. Cavaliere, Econ. J. 4 (2001) 70–88.
[32] C. Castelnovo, A. Podesta, P. Piseri, P. Milani, Phys. Rev. E 65 (2002), 021601/1–021601/11.
[33] N. Scafetta, Paolo Grigolini, Phys. Rev. E 66 (2002), 036130/1–036130/10.
[34] C. Ellis, Phys. A 375 (2007) 159–173.
[35] H.E. Hurst, Trans. Am. Soc. Civil Eng. 116 (1951) 770–808.
[36] B.B. Mandelbrot, J.R. Wallis, Water Resour. Res. 5 (1968) 967–972.
[37] O.I. Yordanov, N.I. Nikolaev, Phys. Rev. E 49 (1994) R2517–R2520.
[38] R. Kant, Phys. Rev. E 53 (1996) 5749–5762.
[39] O.I. Yordanov, I.S. Atanasov, Eur. Phys. J. B 29 (2002) 211–218.
[40] J.J. Wu, Chaos Solitons Fractals 12 (2001) 2481–2492.
[41] T.H. Lan, B.-Q. Xu, H.-J. Yuan, J.-R. Lin, Biophys. Chem. 106 (2003) 67–74.
[42] A. Bru, D. Casero, Europhys. Lett. 64 (2003) 620–626.
[43] L. Ponson, D. Bonamy, E. Bouchaud, Phys. Rev. Lett. 96 (2006), 035506/1–035506/4.
[44] F. Family, T. Vicsek, J. Phys. A 18 (1985) L75–L81.
[45] A.S. Balankin, D. Morales, O. Susarrey, D. Samayoa, J.M. Trinidad, J. Marquez, R. García, Phys. Rev. E 73 (2006), 065105/1–065105/4.
[46] G. Ódor, Rev. Mod. Phys. 76 (2004) 663–724.
[47] J.M. López, M.A. Rodriguez, R. Cuerno, Phys. A 246 (1997) 329–347.
[48] J.J. Ramasco, J.M. López, M.A. Rodriguez, Phys. Rev. Lett. 84 (2000) 2199–2202.
[49] A.S. Balankin, D.M. Matamoros, I. Campos, Philos. Mag. Lett. 80 (2000) 165–172.
[50] A.S. Balankin, D.M. Matamoros, Philos. Mag. Lett. 81 (2001) 495–503.
[51] A.S. Balankin, D.M. Matamoros, Phys. Rev. E 71 (2005), 056102/1–056102/4.
[52] A.S. Balankin, O. Susarrey, R.G. Paredes, L. Morales, Phys. Rev. E 72 (2005), 065101/1–065101/4.
[53] A.S. Balankin, O. Susarrey, R.C. Montes de Oca, D. Samayoa, J.M. Trinidad, M.A. Mendoza, Phys. Rev. E 74 (2006), 061602/1–061602/7.
[54] A.S. Balankin, R.C. Montes de Oca, D. Samayoa, Phys. Rev. E 76 (2007), 032101/1–032101/4.
[55] J. Feder, Fractals, Plenum Press, New York, 1988.
[56] A.S. Balankin, A.D. Izotov, V.U. Novikov, Inorg. Mater. 35 (1999) 1047–1053.
[57] S. Stach, J. Cybo, J. Chmiela, Mater. Charct. 26 (2001) 163–167.
[58] A. Chaudhari, Ch.-Ch. Sanders Yan, Sh.-L. Lee, Appl. Suf. Sci. 238 (2004) 513–517.
[59] A.L. Barabasi, T. Viscek, Phys. Rev. A 44 (1991) 2730–2733.
[60] A.L. Barabasi, M. Jensen, J. Kertész, T. Viscek, Y.Ch. Zang, Phys. Rev. A 45 (1992) R6951–R6954.
[61] J. Asikainen, S. Majaniemi, M. Dubé, T. Ala-Nissila, Phys. Rev. E 65 (2002), 052104/1–052104/4.
[62] J.-S. Gagnon, S. Lovejoy, D. Schertzer, Europhys. Lett. 62 (2003) 801–807.
[63] A.S. Balankin, D.M. Matamoros, Phys. Lett. A 339 (2005) 23–32.
[64] A.S. Balankin, O.M. Matamoros, Phys. Rev. E (2005) 0651061–0651064.
[65] A.S. Balankin, R.G. Paredes, O. Susarrey, D. Morales, F. Castrejon, Phys. Rev. Lett. 96 (2006) 0561011–0561014.
[66] S.J. Mitchell, Phys. Rev. E 72 (2005), R065103/1–R065103/4.
[67] D. Schertzer, S. Lovejoy, Phys. A 92 (1992) 187–194.
[68] S. Ghashghaie, W. Breymann, J. Peinke, P. Talkner, Y. Dodge, Nature 381 (1996) 767–770.
[69] D. Schertzer, S. Lovejoy, J. Appl. Meteorol. 36 (1997) 1296–1303.
[70] J.-S. Gagnon, S. Lovejoy, D. Schertzer, Nonlinear Process. Geophys. 13 (2006) 541–570.
[71] E. Koscielny-Bunde, J.W. Kantelhardt, P. Braun, A. Bunde, Sh. Havlin, J. Geophys. Res. 111 (2006) D01106.
[72] L. Biferale, I. Daumont, A. Lanotte, F. Toschi, Phys. Rev. E 66 (2002), 056306/1–056306/4.
[73] S. Gheorghiu, P. Pfeifer, Phys. Rev. Lett. 85 (2000) 3894–3897.
[74] M. Cevdet, S. Salim, S. Selim, Mater. Res. Bull. 35 (2000) 2165–2172.
[75] Scion Image Beta 4b, http://www.sciocorp.com.
[76] J.B. Bassingthwaighte, G.M. Raymond, Ann. Biomed. Eng. 22 (1994) 432.
[77] D.C. Caccia, D. Percival, M.J. Cannon, G. Raymond, J.B. Basingthwaighte, Phys. A 246 (1997) 609.
[78] R. Weron, Phys. A 312 (2002) 285.
[79] BENOIT 1.3, http://www.trusoft-international.com.